Journal of Electroceramics 3:3, 311–315, 1999

Protonic Conduction in $SrY_{0.5}Ta_{0.5}O_3$-Based Ceramics at Elevated Temperatures

T. SHIMURA, M. SHOJI & H. IWAHARA

Center for Integrated Research in Science and Engineering, Nagoya University, Furo-cho, Chikusa-ku, Nagoya 464-8603, Japan

Submitted December 11, 1998; Revised February 3, 1999; Accepted February 3, 1999

Abstract. The perovskite-type-oxide solid solution $SrY_{0.5+x}Ta_{0.5-x}O_{3-\delta}$ was synthesized and its properties were investigated. The single phase character of the samples was confirmed by X-ray diffraction when $0 \leq x \leq 0.02$, while lines from the impurity phase SrY_2O_4 appeared in patterns of $x \geq 0.03$. The conductivities of $SrY_{0.52}Ta_{0.48}O_{3-\delta}$ were about an order of magnitude higher than those of $SrY_{0.50}Ta_{0.50}O_3$.

The results of electrochemical measurements such as emf measurements of gas concentration cells, isotope effect in conductivity, and oxygen partial pressure dependence of conductivity showed that $SrY_{0.52}Ta_{0.48}O_{3-\delta}$ exhibited pure protonic conduction in reducing atmospheres and *p*-type electronic conduction under high oxygen partial pressure conditions.

Keywords: $SrY_{0.5}Ta_{0.5}O_3$, ordered-perovskite, protonic conduction, concentration cell, isotope effect

Introduction

High temperature protonic conduction was first discovered in perovskite-type $SrCeO_3$-based solid solutions [1]. Since then several perovskite-type oxide solid solution protonic conductors, including $BaCe_{1-x}M_xO_{3-\delta}$ [2], (Ba, Sr or Ca)$Zr_{1-x}M_xO_{3-\delta}$ [3–5], $KTa_{1-x}M_xO_{3-\delta}$ [6], were prepared by many researchers. For the appearance of protonic conduction, they required partial substitution of lower valence dopant element for the B-site ion to introduce oxide ion vacancies in them.

Nowick et al. showed that in some perovskite-type complex oxides, $A_2^{2+}(B^{3+}B'^{5+})O_6$ or $A_3^{2+}(B^{2+}B'^{5+}_2)O_9$, protonic conduction appeared when the B/B' ratio deviates from the stoichiometric value. $Sr(Ga_{0.5+x}Nb_{0.5-x})O_{3-\delta}$, $Sr(Ga_{0.5+x}Ta_{0.5-x})O_{3-\delta}$, $Sr(Nd_{0.5+x}Nb_{0.5-x})O_{3-\delta}$, [7] and $Sr(Sc_{0.5+x}Nb_{0.5-x})O_{3-\delta}$ [8] belong to these types of protonic conductors. Also $Ba_3(Ca_{1.18}Nb_{1.82})O_{9-\delta}$ (BCN18)[8] belong to this kind of perovskite-type, and much attention has been paid to this material because of its high conductivity [9–13].

In this paper, we report the transport properties of $Sr(Y_{0.5+x}Ta_{0.5-x})O_{3-\delta}$. The crystal structure of stoichiometric $Sr(Y_{0.5}Ta_{0.5})O_3$ was already reported [14], but the conduction properties of $Sr(Y_{0.5}Ta_{0.5})O_3$-based non-stoichiometric compounds have not been investigated yet. The result of this investigation will provide this information and will aid in understanding of proton conduction phenomena in perovskite-based compounds.

Experimental

Samples were prepared by the conventional solid state reaction method using $SrCO_3$, Y_2O_3 and Ta_2O_5 as starting materials. Required amounts of starting materials were mixed in an agate mortar with ethanol and then calcined at 1200°C. Furnace-cooled sample powder was grounded by ball milling and then pressed into a pellet having diameter of 13 mm. This pellet was sintered at 1670°C for 10 h and cooled to room temperature in the furnace.

The phase contents of the samples were examined by powder X-ray diffraction analysis (XRD). The conductivities of the samples were measured as a function of temperature and atmosphere. The ac impedance method (solartron 1260 gainphase/impedance analyzer) was used for the conductivity measurement. To determine the ionic conduction properties, the open circuit emfs of gas concentration cells using the specimens as the electrolyte were measured. The effect of D_2 in the atmosphere on conductivity was also measured.

Results and Discussions

Figure 1 shows the XRD patterns of $SrY_{0.5+x}Ta_{0.5-x}O_{3-\delta}$ ($0 \leq x \leq 0.03$). Single phase samples were obtained for $0 \leq x \leq 0.02$. At $0 \leq x \leq 0.02$, all diffraction peaks could be indexed for the cubic perovskite lattice having the rock-salt type order of B-site ions, the lattice constant of $SrY_{0.52}Ta_{0.48}O_{3-\delta}$ being 0.8226(5) nm. The reported rhombohedral distortion in $SrY_{0.5}Ta_{0.5}O_3$ [14] was not observed in the work. Since at $x = 0.03$ two small peaks from the impurity phase SrY_2O_4 appeared in the diffraction patterns (indicated by arrows), the upper limit of x which gave single phase region appeared to be between 0.02 and 0.03. This limit was apparently lower than those in $Sr(Ga_{0.5+x}Nb_{0.5-x})O_{3-\delta}$ ($x = 0.1$), $Sr(Ga_{0.5+x}Ta_{0.5-x})O_{3-\delta}$ ($x = 0.05$), $Sr(Nd_{0.5+x}Nb_{0.5-x})O_{3-\delta}$ ($x = 0.05$) [7] and $Sr(Sc_{0.5+x}Nb_{0.5-x})O_{3-\delta}$ ($x = 0.05$) [8].

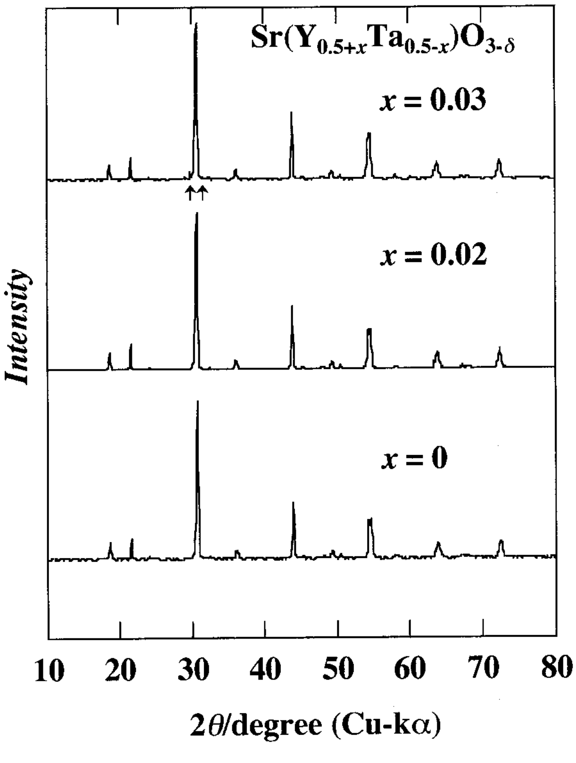

Fig. 1. XRD patterns of $SrY_{0.5+x}Ta_{0.5-x}O_{3-\delta}$ ($x = 0$, 0.02 and 0.03) at room temperature. Arrows indicates the diffraction lines from the impurity phase SrY_2O_4.

The ionic radii of six coordinated Y^{3+} and Ta^{5+} are 0.090 nm and 0.064 nm, [15] respectively. The large difference in radii between them, 0.026 nm, is the origin of ionic ordering on the B-site [7]. $Sr(Nd_{0.5}Nb_{0.5})O_3$ also has B-site ordering due to the large difference of ionic radii. No ordering was detected in $Sr(Ga_{0.5}Nb_{0.5})O_3$, $Sr(Ga_{0.5}Ta_{0.5})O_3$ and $Sr(Sc_{0.5}Nb_{0.5})O_3$. The ordering of the B-site ions in $SrY_{0.5}Ta_{0.5}O_3$ is apparently a disadvantage for Y^{3+} substitution for Ta^{5+}, since it is difficult for the large Y^{3+} to enter into the small Ta-site (TaO_6 octahedron).

Figure 2 shows the temperature dependence of conductivities of $SrY_{0.5+x}Ta_{0.5-x}O_{3-\delta}$ ($x = 0$ and 0.02) in wet air and in wet hydrogen. It is clear that with increasing x the conductivities increase, although the conductivities of $SrY_{0.52}Ta_{0.48}O_{3-\delta}$ are not so high. In $SrY_{0.52}Ta_{0.48}O_{3-\delta}$, the activation energy for conduction in wet hydrogen is about 0.85 eV, which is clearly lower than that in wet air, about 1.42 eV. This large difference in activation energies suggests that there is a difference in conduction mechanism between that in air and in hydrogen. To investigate the conduction properties in detail, the dependence of the conductivity on oxygen partial pressure was measured at 800 and 1000°C. Figure 3 shows the results. At 1000°C, there is a clear oxygen partial pressure dependence of conductivity at high P_{O_2}. The slope, $\partial \log\sigma/\partial \log P_{O_2}$, is close to 1/4, suggesting that holes generated by the following reaction are the dominant conductive carriers.

$$V_O^{\bullet\bullet} + 1/2O_2 = O_O^{\times} + 2h^{\bullet} \qquad (1)$$

The high activation energy in air, thus, might represent the high activation energy of hole generation and migration.

On the other hand, there is only a weak dependence at 800°C. At 800°C, the conduction under high P_{O_2} might be ionic.

At $P_{O_2} < 10^{-7}$ atm, there is nearly no oxygen partial pressure dependence of conductivity at both

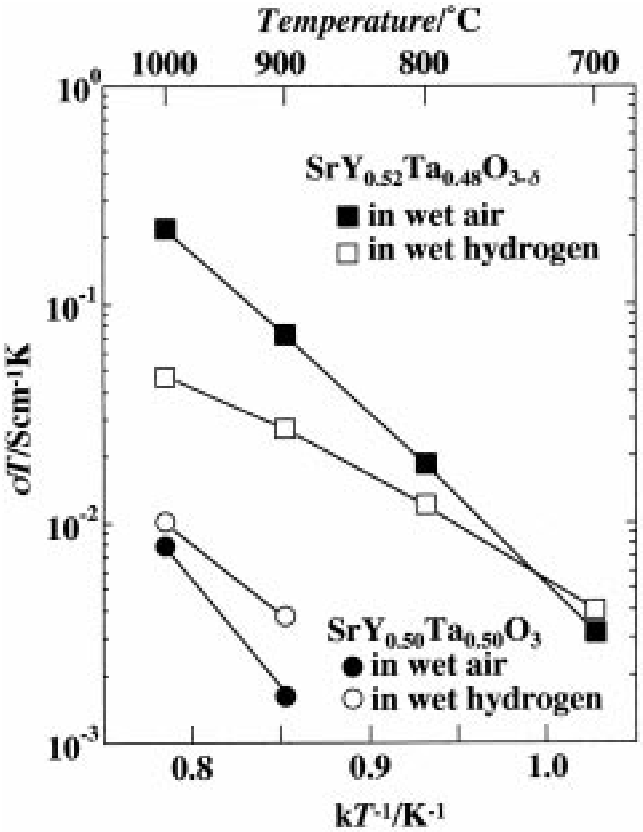

Fig. 2. The Electrical conductivities of $SrY_{0.5+x}Ta_{0.5-x}O_{3-\delta}$ ($x = 0$ and 0.02) in wet air (close symbols) and in wet hydrogen (open symbols).

800 and 1000°C, thereby showing no evidence for *n*-type electronic conduction.

To investigate the ionic species conduction under low oxygen partial pressure condition, the H/D isotope effect on conductivity was measured at 600–1000°C. Figure 4 shows the conductivities of $SrY_{0.52}Ta_{0.48}O_{3-\delta}$ measured in D_2 gas saturated with D_2O and those in wet H_2. Since another sample was used for this experiment, conductivities in H_2 shown in Fig. 4 are not precisely the same as those shown in Fig. 2. However, the activation energies of both conductivities showed good agreement. From the result shown in Fig. 4, it is apparent that conductivities in D_2 are lower than those in H_2. The ratios, $\sigma H_2/\sigma D_2$, are about 1.3–1.7 at each measured temperature. These values are close to $\sqrt{2}$, which is the estimated ratio of $\sigma H_2/\sigma D_2$ based on the simple ion hopping conduction model. This result supports the choice of H^+ or D^+ as the dominant conductive ionic species.

The result of the conductivity measurements with changing oxygen partial pressure showed that $SrY_{0.52}Ta_{0.48}O_{3-\delta}$ has a high ionic transport number in reducing atmospheres, even at 1000°C. This is an important feature for sensor applications.

To confirm the high transport number in reducing atmospheres, the hydrogen concentration cell using this oxide as a solid electrolyte,

$$\text{wet } H_2(1\text{ atm}),\text{Pt} \mid SrY_{0.52}Ta_{0.48}O_{3-\delta} \mid \text{Pt, wet Ar-}H_2\ (P_{H_2})$$

was constructed and its emfs were measured. Figure 5 shows the results at 700, 800, 900 and 1000°C. The dashed lines represent the theoretical Nernst emfs at each temperature.

It is apparent that the experimental emfs accurately match the theoretical values. This means that the transport number of ions is unity between 700 and 1000°C, as expected.

Figure 6 shows the emfs of the oxygen concentration cell,

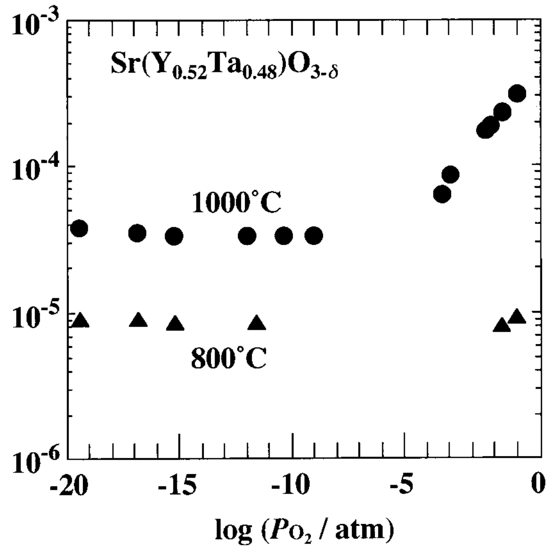

Fig. 3. The dependence of conductivity of $SrY_{0.52}Ta_{0.48}O_{3-\delta}$ on oxygen partial pressure at 800 and 1000°C.

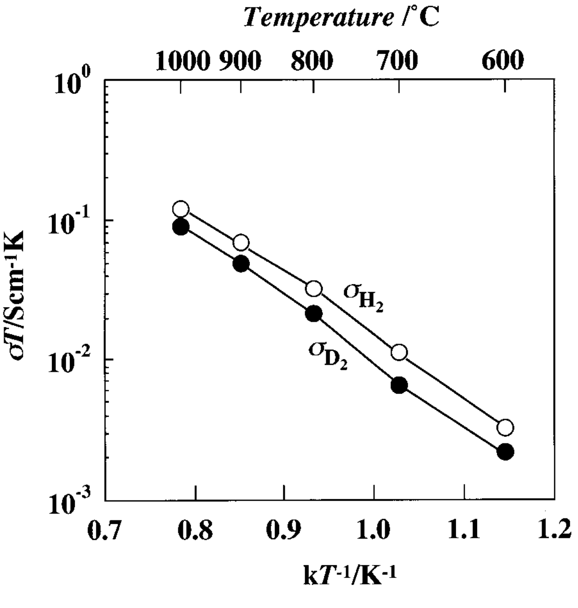

Fig. 4. The H/D isotope effect on conductivity of $SrY_{0.52}Ta_{0.48}O_{3-\delta}$.

$$\text{dry air, Pt} \mid SrY_{0.52}Ta_{0.48}O_{3-\delta} \mid \text{Pt, dry } O_2$$

at 700 to 1000°C. The dry gases used here were prepared by passing them through a dry ice-ethanol cold trap. The emfs of this oxygen concentration cell are zero. However, at least below 800°C, the

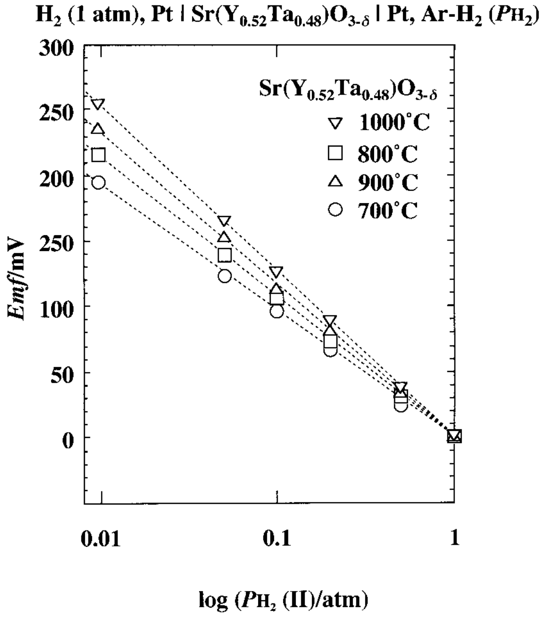

Fig. 5. The measured emfs of a hydrogen concentration cell using $SrY_{0.52}Ta_{0.48}O_{3-\delta}$ as a solid diaphragm at 700, 800, 900 and 1000°C. Dashed lines express the theoretical emfs at each temperature.

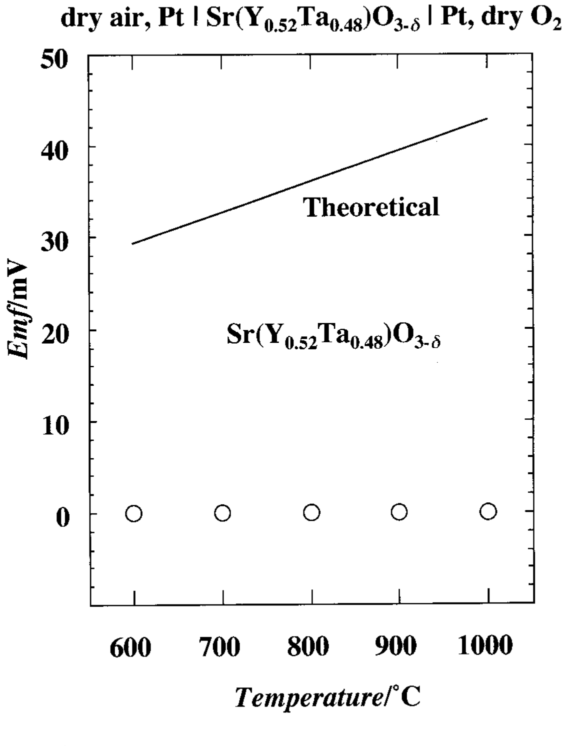

Fig. 6. The emfs of an oxygen concentration cell using $SrY_{0.52}Ta_{0.48}O_{3-\delta}$ as a solid diaphragm between 600 and 1000°C. Straight line represents the theoretical emfs.

dependence of the conductivity on oxygen partial pressure measured under wet condition (shown in Fig. 3) suggests some ionic contribution at high P_{O_2}. This means that when there is no proton source in the atmosphere, $SrY_{0.52}Ta_{0.48}O_{3-\delta}$ shows no ionic conduction.

As shown above, $SrY_{0.52}Ta_{0.48}O_{3-\delta}$ is a pure protonic conductor at high temperature, although conductivity is not higher than for other protonic conductors. One reason for this low conductivity might be the low concentration of oxide ion vacancies. Cationic ordering at the B-site may not be a serious problem. $Ba_3(Ca_{1.18}Nb_{1.82})O_{9-\delta}$ (BCN 18) shows high conductivity in spite of 1:1 ordering at the B-site [11]. Another possible reason for the low conductivity might be the low basicity of the component cations, which would result in the low solubility of protons [5].

Conclusion

Perovskite-type complex oxides, $SrY_{0.5+x}Ta_{0.5-x}O_{3-\delta}$, were synthesized and their high temperature conduction properties were measured. Single phase character was confirmed for $0 \leq x \leq 0.02$ from XRD and the super lattice diffractions in XRD indicated cationic order on the B-site. The conductivity increased with increasing x. In reducing atmosphere, the H/D isotope effect clearly appeared in the conductivity. Between 700 and 1000°C, the emfs of the hydrogen concentration cell were equal to the theoretical values, whereas the emfs of the oxygen concentration cell were zero. These results indicate that in hydrogen, $SrY_{0.52}Ta_{0.48}O_{3-\delta}$ is a pure protonic conductor whose transport number is unity, and there is no contribution of oxide ions to conduction under high P_{O_2} conditions.

Acknowledgment

The authors wish to express their thanks to grant-in-aid from the Ministry of Education, Science and Culture, Japan, (Fundamental Research-A, No. 10305048).

References

1. H. Iwahara, T. Esaka, H. Uchida, and N. Maeda, *Solid State Ionics*, **3/4**, 359 (1981).
2. H. Iwahara, H. Uchida, K. Ono, and K. Ogaki, *J. Electrochem. Soc.*, **135**, 529 (1988).
3. T. Yajima, H. Kazeoka, T. Yogo, and H. Iwahara, *Solid State Ionics*, **47**, 271 (1991).
4. T. Yajima, H. Suzuki, T. Yogo, and H. Iwahara, *Solid State Ionics*, **51**, 101 (1992).
5. H. Iwahara, T. Yajima, T. Hibino, K. Ozaki, and H. Suzuki, *Solid State Ionics*, **61**, 65 (1993).
6. W.-K. Lee and A.S. Nowick, *Solid State Ionics*, **18/19**, 989 (1986).
7. K.C. Liang and A.S. Nowick, *Solid State Ionics*, **61**, 77 (1993).
8. K.C. Liang, Y. Du, and A.S. Nowick, *Solid State Ionics*, **69**, 117 (1994).
9. A.S. Nowick, *J. Amer. Cer. Soc.*, **78**, 3033 (1995).
10. M. Pinoke, T. Mono, W. Schweika, T. Springer, and H. Schober, *Solid State Ionics*, **97**, 497 (1997).
11. E. Zimmer, K. Scharf, T. Mono, J. Friedrich, and T. Schober, *Solid State Ionics*, **97**, 505 (1997).
12. S. Valkenberg, H.G. Bohn, and W. Schilling, *Solid State Ionics*, **97**, 511 (1997).
13. S. Bausch, H.G. Bohn, and W. Schilling, *Solid State Ionics*, **97**, 517 (1997).
14. M.F. Kupriyanov and V.S. Fillipev, *Kristallografiya*, **8**, 356 (1963).
15. R.D. Shannon, *Acta Crysallogr.*, **32**, 751 (1976).